Title: Effects of basal clearance on the impact dynamics of dry granular flow against dual rigid barriers

Authors: Charles W. W. Ng; Haiming Liu*; Clarence E. Choi; Aastha Bhatta; Min Zheng

First-author
Name: Dr Charles Wang Wai Ng
Affiliation: Department of Civil and Environmental Engineering, The Hong Kong University of Science and Technology
Address: The Hong Kong University of Science and Technology, Clear Water Bay, Kowloon, Hong Kong, China
Email: charles.ng@ust.hk

Corresponding author*
Name: Dr Haiming Liu
Affiliation: Department of Civil and Environmental Engineering, The Hong Kong University of Science and Technology
Address: The Hong Kong University of Science and Technology, Clear Water Bay, Kowloon, Hong Kong, China
Email: hliubc@connect.ust.hk
Tel: +852 54498463

Co-author
Name: Dr Clarence Edward Choi
Affiliation: 1. Department of Civil Engineering, The University of Hong Kong; 2. The University of Hong Kong Shenzhen Institute of Research and Innovation
Address: 1. The University of Hong Kong, Pokfulam Road, Hong Kong, China; 2. The University of Hong Kong Shenzhen Institute of Research and Innovation, Nanshan, Shenzhen, China
Email: cechoi@hku.hk

Co-author
Name: Miss Aastha Bhatta
Affiliation: Department of Civil and Environmental Engineering, The Hong Kong University of Science and Technology
Address: The Hong Kong University of Science and Technology, Clear Water Bay, Kowloon, Hong Kong, China
Email: abhatta@connect.ust.hk

Co-author
Name: Miss Min Zheng
Affiliation: Department of Civil and Environmental Engineering, The Hong Kong University of Science and Technology
Address: The Hong Kong University of Science and Technology, Clear Water Bay, Kowloon, Hong Kong, China
Email: mzhengaj@connect.ust.hk

Effects of basal clearance on the impact dynamics of dry granular flow against dual rigid barriers

Charles W. W. Ng; Haiming Liu*; Clarence E. Choi; Aastha Bhatta; Min Zheng
*Corresponding author

ABSTRACT: A basal clearance is usually designed beneath barriers to enable sufficient discharge to minimise the maintenance work over service life. Current design guidelines for multiple barriers usually neglect the influence of basal clearance, resulting in either an over-conservative or a non-conservative design impact force acting on the subsequent barriers. In this study, physical model tests were carried out to investigate the effects of basal clearance height (H_c) beneath first barrier on the interaction between dry granular flow and dual rigid barriers. A new approach based on the hydrodynamic equation is proposed to estimate the impact force on the second barrier exerted by the basal discharge and overflow from the first barrier. The basal discharge can attenuate the impact force exerted on the second barrier by dissipating the kinetic energy of landing flow and apportioning the load contributions from basal discharge and overflow. For the first barrier with a barrier height H_{B1} that was twice of the flow depth h_0, the impact force on the second barrier was governed by overflow when $H_c/h_0 \leq 0.6$ and was dominated by basal discharge when $H_c/h_0 \geq 0.8$. These two criteria provide a basis for optimising the impact forces for multiple-barrier systems with basal clearances.

Keywords: basal clearance; impact; overflow; dual rigid barriers; physical modelling

Introduction

Compared with the use of a single and large terminal barrier at the end of a catchment (Kwan 2012), multiple barriers can progressively arrest debris and dissipate debris energy by creating a cascading effect (Wendeler et al. 2008; WSL 2008; Ng et al. 2019). Barriers in the field are usually designed with a basal clearance (Wendeler et al. 2008, 2019; Volkwein 2014; Piton and Recking 2016; Choi et al. 2020), which is an opening between channel bed and the base of the barrier, to enable discharge. A basal clearance can minimise the accumulation of the stream loads to reduce the maintenance (Chiari et al. 2016; Sze and Lam 2017; Morstabilini et al. 2019) of the barriers and ensure that multiple barriers can resist the designed flow volume. Additionally, a basal clearance can regulate the peak flow discharge (Nagl et al. 2016; Morstabilini and Deana 2019) and therefore optimise the impact forces of multiple barriers. Despite the engineering value of a basal clearance, existing design guidance is mainly empirical.

Physical model tests using a flume for closed dual rigid barriers have been conducted by Ng et al. (2018; 2019; 2021) to investigate the overflow and landing dynamics and the impact force on the second barrier. However, the impact dynamics of flow against multiple barriers with basal clearance have yet to be elucidated. Choi et al. (2020) carried out a series of physical experiments to investigate the impact dynamics of dry granular flow against a single rigid barrier with a basal clearance. In their study, a tall enough barrier was installed to prevent overflow and the effects of basal clearance and barrier height on the impact force of the second barrier were not studied. However, neglecting the effects of basal clearance and barrier height on the impact force of second barrier can result in not only an overly conservative design but also a non-conservative design due to the larger impact force that may be caused by the basal discharge and overflow. The necessity of designing a basal clearance to ensure a conservative design highlights the importance of studying the effects of basal clearance on the impact dynamics of flow against multiple barriers.

An analytical framework for the design of multiple barriers was proposed and evaluated by Kwan et al. (2015) and Ng et al. (2018; 2019). Figure 1 shows a schematic of the interaction mechanisms between debris flow and two rigid barriers. When flow impacts the first barrier, flow is redirected upwards and deposition accumulates to the crest of the barrier. Subsequently, overflow with a velocity v_m launches over the crest of the barrier. The overflow trajectory can be approximated as a point mass. The overflow distance can be expressed as follows:

$$x_i = \frac{v_m^2}{g\cos\theta}\left[\tan\theta + \sqrt{\tan^2\theta + \frac{2gH_{B1}}{v_m^2\cos\theta}}\right] + H_{B1}\tan\theta \quad (1)$$

The flow velocity before landing can be obtained by assuming the energy of the point mass is conserved and is given as follows:

$$v_r = \sqrt{v_m^2 + 2g(H_{B1}\cos\theta + x_i\sin\theta)} \quad (2)$$

After the debris lands on the bed, the energy of the flow is attenuated. A landing factor C_r can serve to quantify the energy dissipation when overflow lands on a bed. The C_r can be varied by the flow composition and the channel bed materials at the landing location (Yang et al. 2011; Glassey 2013; Kwan et al. 2015). Additionally, the C_r may be affected by the Froude number of the incoming flow and the ratio between barrier height and flow depth by altering the flow run-up and impact processes (Hákonardóttir et al. 2003; Faug et al. 2012; Faug 2015). The changed impact dynamics may in turn change the launching and landing angles and result in different C_r (Ng et al. 2019). Kwan et al. (2015) reviewed field monitoring data of debris flows and flume test results for both dry granular flows and debris flows at slope angles from 5° to 26°. The dry granular flows in the flume tests had a Froude number of 3 and the ratio between barrier height and flow depth ranged from 1.1 to 2.5. They found that the landing factor ranged from 0.5 to 0.7 for debris landing on a hard bed, while the landing factor varied from 0.3 to 0.5 for a soft bed composed of filled debris. To consider the uncertainties that are

involved during the complex landing process, they recommended C_r = 0.7. With the recommended landing factor, the flow velocity after landing is given as follows:

$$v_i = C_r v_r \tag{3}$$

Based on the velocity after landing, the impact force on the next barrier in the channel can be estimated using the hydrodynamic equation (Hübl et al. 2009; Armanini et al. 2011):

$$F = \alpha \rho v^2 h_0 w \tag{4}$$

The abovementioned analytical framework is for closed barrier without any openings and the effects of a basal clearance are not considered. Figure 2 shows a schematic of the interaction between the flow and dual rigid barriers with a basal clearance underneath the first barrier. The first barrier has a distance from the top of the barrier to the channel bed of H_1, which composes of barrier height H_{B1} and a basal clearance height H_c. When the flow event is small and overflow does not occur (Fig. 2*a*), the flow discharges through the basal clearance and impacts the second barrier. For a large event, the flow first discharges through the basal clearance and eventually overflows the barrier (Fig. 2*b*). Evidently, the presence of a basal clearance will alter the impact dynamics on the first and second barriers.

In this study, a series of tests were carried out with a 5-m-long flume to investigate the impact mechanisms of dry granular flow on dual rigid barriers with varying basal clearances beneath the first barrier. The effects of first barrier height on the impact force of second barrier are also examined by allowing and not allowing overflow from the first barrier. New analytical equations are proposed and evaluated to estimate the impact force of basal discharge and overflow on the second barrier.

New analytical equations for estimating the impact force of basal discharge and overflow on the second barrier

Impact force of basal discharge

When flow interacts with a rigid barrier that has a basal clearance, the flow is resisted by the barrier only when the flow depth is larger than the basal clearance. By assuming the initially discharged flow transports to downstream as a point mass, the velocity of the discharge flow can be expressed as:

$$v_{\mathrm{d}} = \sqrt{v_1^2 + 2Lg(\sin\theta - \tan\varphi\cos\theta)} \tag{5}$$

where v_1 is the frontal velocity of the flow reaching the first barrier location, L is the transportation distance away from the first barrier, and φ is the interface friction angle between the flow and the channel base. When flow propagating to downstream, we assume that the discharge flow depth is a function of basal clearance and is expressed as follows:

$$h_{\mathrm{d}} = \xi H_{\mathrm{c}} \tag{6}$$

Substituting eqs. (5) and (6) into eq. (4), the impact force of discharge flow on the second barrier with barrier spacing of L_{s} is given as follows:

$$F_{\mathrm{d}} = \alpha\rho\xi H_{\mathrm{c}} w[v_1^2 + 2L_{\mathrm{s}}g(\sin\theta - \tan\varphi\cos\theta)] \tag{7}$$

Impact force of overflow

For rigid barrier with a basal clearance, the impact velocity v_{Hc} on the barrier can be taken as the velocity when flow depth reaches the basal clearance based on the hydrographs of flow depth and flow velocity at the barrier location. Overflow velocity can be obtained by simply assuming energy conservation and the frictional energy dissipation occurs between the flow and the barrier face during the run-up process. The overflow velocity can be expressed as

follows:

$$v_{\mathrm{m}} = \sqrt{v_{\mathrm{Hc}}^2 - 2gH_{\mathrm{B1}}(\cos\theta + \sin\theta\tan\varphi)} \tag{8}$$

Substituting eq. (8) into eqs. (2) and (3) yields:

$$v_{\mathrm{i}} = C_{\mathrm{r}}\sqrt{v_{\mathrm{Hc}}^2 + 2g\sin\theta(x_{\mathrm{i}} - H_{\mathrm{B1}}\tan\varphi)} \tag{9}$$

Assuming the impact force of overflow is dominated by the velocity after landing and the flow depth at the first barrier location, the impact force of overflow is given as follows:

$$F_{\mathrm{L}} = \alpha\rho h_0 w C_{\mathrm{r}}^2[v_{\mathrm{Hc}}^2 + 2g\sin\theta(x_{\mathrm{i}} - H_{\mathrm{B1}}\tan\varphi)] \tag{10}$$

Impact force from combined basal discharge and overflow

To estimate the peak impact force on the second barrier from combined basal discharge and overflow, the run-up height of the flow against the first barrier should be first examined to determine the occurrence of overflow. The run-up of the flow can be calculated by the design approach recommended by Kwan (2012) for rigid barrier without opening for a conservative prediction.

If the run-up height of the flow is lower than the first barrier height, eq. (7) can be adopted to estimate the peak impact force of second barrier. Otherwise, the peak impact force on the second barrier can be determined by the larger impact force from basal discharge and overflow calculated by eqs. (7) and (10) and is expressed as follows:

$$F_{\mathrm{T}} = \max\{\alpha\rho\xi H_{\mathrm{c}} w\left[v_1^2 + 2L_{\mathrm{s}}g(\sin\theta - \tan\varphi\cos\theta)\right], \alpha\rho h_0 w C_{\mathrm{r}}^2[v_{\mathrm{Hc}}^2 + 2g\sin\theta(x_{\mathrm{i}} - H_{\mathrm{B1}}\tan\varphi)]\} \tag{11}$$

Flume modelling

The experiments were carried out in a rectangular flume model. The flume had a total length of 5 m, a width of 0.2 m and a depth of 0.5 m. The sidewalls and channel bed were made up of

10-mm-thick acrylic plates reinforced by steel frames. The storage container at the upstream of the flume had a length of 0.5 m to retain the test material with a gate. A pneumatic device was installed on the flume to control the gate. The pneumatic device was activated during the test to lift the gate and release all the source material down the flume.

Scaling and flow characterisation

Froude number is ratio between flow inertial force and gravitational force and is expressed as $Fr = v/\sqrt{gh_0\cos\theta}$. Froude number is an essential parameter for correlating the dynamics of open-channel flows and their resulting impact force on barriers (Armanini et al. 2011; Choi et al. 2016, 2017; Hübl et al. 2009; Faug 2015; Ng et al. 2017*a*, 2017*b*). In this study, the Froude number of the flow before impacting the first barrier was targeted at $Fr = 3$, which lies within the range of typical flows in the field (Arattano et al. 1997; Hübl et al. 2009; Ng et al. 2013, 2018). Iverson et al. (2004) and Iverson (2015) illustrated that small-scale experiments are appropriate to model cohesionless dry granular flows because the pore air of the flows has negligible scaling effects on flow dynamics. Therefore, modelling uniform dry granular flow serves as an idealised case for natural geophysical flows, such as debris and rock avalanches, where pore fluid is air.

Instrumentation

Figure 3 shows a side schematic of the flume and instrumentation. Two rigid barriers were installed 1100 mm and 2500 mm away from the gate of the storage container. The second barrier was composed of a supporting barrier that was fixed with the sidewalls of the flume and a force plate made of a 15-mm-thick acrylic board. A load cell was sandwiched between the support barrier and the force plate to measure the impact force exerted by the flow. Two high-

speed cameras were installed at the side of the flume to capture the impact kinematics and estimate the flow velocity and depth. A video camera was mounted between the dual barriers to capture an overall side view of the interaction between flow and dual barriers. The high-speed cameras recorded images at 400 frames per second with a resolution of 1696 pixels × 982 pixels. The video camera had a sampling rate of 120 frames per second at a resolution of 1920 pixels × 1080 pixels. Two ultrasonic sensors were mounted along the centreline above the flume to measure the flow depth after impacting the first barrier. The distances of the two ultrasonic sensors to the gate were 1400 mm and 2200 mm to obtain flow depths near first and second barriers, respectively.

Test programme

Spherical glass beads with a uniform diameter of 3 mm and a total mass of 50 kg were adopted in this study. The test material had a bulk density of 1620 kg/m^3 and a dynamic friction angle of 18º (Ng et al. 2017*b*). Some of the glass beads were dyed black to facilitate a clear observation of flow kinematics. Control test without installing any barrier was first carried out to characterise the Froude number at the first barrier location. After control test, flume inclination was chosen as 25º and the first barrier was installed 1100 mm away from the storage gate to obtain a Froude number of 3, which was determined by the frontal flow velocity (2.1 m/s) and the maximum flow depth (48 mm).

The maximum flow depth and the frontal flow velocity were measured by the high-speed camera images that captured a side view of the flow kinematics with a reference grid of 50 mm in size on the sidewall of the flume. The frontal flow velocity was measured following a similar approach reported by Ashwood and Hungr (2016). Since the dilute flow front had a much higher velocity and was not representative of the flow momentum, the frontal velocity is determined by the average velocity of the subsequent thicker portion of the flow passing from

50 mm upstream to 50 mm downstream of the first barrier location (Choi et al. 2020). The time history of the flow depth was also measured by an ultrasonic sensor mounted above the centre of the first barrier location as shown in Fig. 4. The results obtained by the ultrasonic sensor indicate that the flow depth at the centre of the flow is almost the same as the measured flow depth from the sidewall. Following the same approach to estimate the flow frontal velocity, the time history of the flow velocity was measured every 0.1 s and is shown in Fig. 4. The frontal velocity is nearly 20% higher than the flow velocity with maximum flow depth, indicating that the Froude number with frontal velocity is also around 20% higher than the Froude number using maximum flow depth with its corresponding flow velocity. Nevertheless, using the frontal velocity together with the maximum flow depth under free-field conditions serves as a conservative estimation of the impact dynamics. The same free-field approach is usually adopted to obtain the velocity and flow depth for barrier design in Hong Kong (Kwan 2012; Kwan and Koo 2015).

Later, the tests with dual rigid barriers were carried out. To discern the effects of basal discharge and overflow on the interaction between flow and dual barriers, first barrier heights of 100 mm and 500 mm were adopted in this study to allow and not allow overflow, respectively. The barrier height of 100 mm was chosen as suggested by Ng et al. (2018) that a barrier height should be larger than twice of the maximum flow thickness to optimise the design of second barrier. The basal clearance H_c beneath the first barrier was varied from 10 mm to 40 mm with a ratio between H_c and maximum flow depth at the first barrier H_c/h_0 ranging from 0.2 to 0.8. For the short first barrier, a test without basal clearance was also carried out as a reference test. The total height of the first barrier H_1 is the distance from the top of the barrier to the channel bed. The two types of first barrier had a total height of 100 mm to 140 mm and 510 mm to 540 mm, respectively. The second barrier had a height H_{B2} of 260 mm without any basal clearance to resist all the flow material and was placed 1400 mm downstream the first

barrier. This barrier spacing was selected to allow a relative far travelling distance for flow after landing so that the flow depth and flow velocity along the transportation can be obtained. A detailed test programmed is summarised in Table 1.

Test procedures

The glass beads with total mass of 50 kg was loaded into the storage container before each test. Afterwards, the flume was inclined to the target angle 25º. The load cells and ultrasonic sensors were triggered by a data logger and cameras were started. The gate of the storage container was lifted up to release all the test material.

Interpretation of test results

Observed impact kinematics on the first barrier

Figure 5 shows the observed impact kinematics captured by the high-speed camera (left) and the flow velocity fields (right) analysed using the particle image velocimetry (PIV) method (Thielicke 2014; Thielicke and Stamhuis 2014) for test B1C3, where the first barrier had a normalised basal clearance of 0.6 and a normalised barrier height of 2 to allow both overflow and basal discharge. Noted that the fisheye effect of the high-speed camera resulted in a distortion to the captured images as indicated by the distorted grids that had a uniform size of 50 mm by 50 mm. By examining the sizes of the distorted grids, the average grid size was adopted for PIV analyses. The maximum and minimum distorted grid sizes were 7% and 6% different from the average grid size, respectively. Therefore, the image distortion may induce an error of the PIV analysis by around 7% (Pudasaini and Hutter 2007). The PIV results were compared with the measured maximum velocities by high-speed camera and had an error ± 0.2 m/s.

At time t = 0.00 s, the flow front reached the first barrier and discharged through the

basal clearance. The flow impacted the base of the barrier as the depth of the tapered flow front became larger than the clearance at t = 0.20 s (Fig. 5*a*). Some flow was then redirected along the impact face of the barrier and accumulated along the barrier (Fig. 5*b*). Incoming granular flow impacted and rode on top of the accumulated deposit, while some of the deposits near the clearance is observed to discharge underneath the barrier. From the PIV analysis, an interface between the incoming flow and the quasi-static zone is observed. Shearing between the incoming flow and accumulated material noticeably decelerated the flow. The measured maximum flow velocity reduced from 1.8 m/s to 1.1 m/s, indicating the dissipation of flow kinetic energy. At t = 0.62 s (Fig. 5*c*), overflow accelerated to a maximum velocity of 1.9 m/s due to a gain in kinetic energy from the conversion of potential energy and started to land on the basal discharge with a smaller velocity than the landing flow. The accumulated debris behind the barrier continued to enlarge as the momentum flux of the debris from the storage container decreased due to limited supply of granular material. As the debris landed on the channel, the flow velocity decreased and velocity vector changed to a slope-parallel direction (Fig. 5*d*). As overflow continued to cascade over the first barrier, an accumulation of debris is observed at the point of landing. PIV analysis shows a velocity reduction at landing, indicating that the granular material on the channel bed before the overflow impact serves to attenuate the flow kinetic energy. The energy attenuation may be mainly because the basal discharge had lower velocity compared with the landing velocity. Consequently, the basal discharge resisted the landed flow and induced more energy dissipation compared with no basal discharge condition. The attenuation on flow kinetic energy after landing also implies that a different landing factor C_r as expressed in eq. (3) may need to be considered when there is basal discharge.

Observed impact kinematics on the second barrier

Figure 6 shows the observed impact kinematics captured by the normal video camera for test B1C4, where the normalised basal clearance beneath the first barrier was 0.8 and the normalised barrier height was 2. At t = 0.62 s (Fig. 6*a*), the basal discharge reached the second barrier and the overflow of the first barrier did not land yet. At t = 0.93 s, the basal discharge impacted on the second barrier and the overflow from the first barrier landed on the basal discharge (Fig. 6*b*). The combination of basal discharge and overflow flowed downstream and impacted on the second barrier (Fig. 6*c*). The initially arrested basal discharge by the second barrier formed a deposition and shielded the barrier from subsequent impact (Fig. 6*c*). With incoming basal discharge and overflow from the first barrier, the deposited material behind the second barrier continued to accumulate and pileup in the upstream direction (Fig. 6*d*), eventually reaching the first barrier and blocking any further discharge from the clearance of the first barrier (Fig. 6*e*).

The observed impact kinematics of the second barrier indicate that the presence of a basal clearance can apportion the impact force on the second barrier from basal discharge and overflow of the first barrier. The overflow impact force on the second barrier may be attenuated by landing on the basal discharge and impacting on the deposited basal discharge which is arrested by the second barrier.

The jamming observed in Fig. 6*e* implies that a barrier with basal clearance can resume flow retention once the downstream deposition reaches the basal clearance. Evidently, the barrier spacing and basal clearance need to be properly designed to enable the basal clearance to discharge all the retained material to downstream and minimise the maintenance required for the barrier. A relationship between jamming by the second barrier deposition and barrier spacing is discussed in the following section.

Requirement of barrier spacing and basal clearance for preventing jamming

The jamming or the blockage of a basal clearance will render it ineffective. Thus, criteria are discussed in this section for determining the barrier spacing required so that the accumulation of debris from the second barrier does not eventually block the clearance of the first barrier.

The deposition profile of the debris behind the second barrier is largely governed by the spacing between barriers, height of barrier and angle of repose of the debris (VanDine 1996). Figure 7 shows a schematic of the condition where the clearance of the first barrier becomes blocked. For flow material that has an angle of repose less than the slope angle, the deposition thickness decreases from the second barrier to the first barrier (Fig. 7*a*). Based on geometry, the deposition thickness H_{dh} at the first barrier can be expressed as follows:

$$H_{\mathrm{dh}} = H_{\mathrm{B2}} - L_{\mathrm{s}}\tan(\theta - \varphi) \tag{12}$$

It is assumed that the basal clearance of the first barrier can be blocked only if the deposition height at the first barrier is equal or larger than the clearance height, more specifically when $H_{\mathrm{dh}} \geq H_{\mathrm{c}}$. When $H_{\mathrm{c}} > H_{\mathrm{B2}}$, the downstream deposition thickness will be always smaller than the basal clearance and therefore blockage will not occur. When $H_{\mathrm{c}} \leq H_{\mathrm{B2}}$, the minimum spacing required to prevent blockage can be obtained by assuming $H_{\mathrm{dh}} = H_{\mathrm{c}}$:

$$L_{\mathrm{cs}} = \frac{H_{\mathrm{B2}} - H_{\mathrm{c}}}{\tan(\theta - \varphi)} \tag{13}$$

When the barrier spacing is larger than L_{cs}, the basal clearance of the first barrier will not be blocked by the debris that accumulates behind the second barrier.

Figure 7*b* shows the deposition profile when the angle of repose of the flow material is equal to or larger than the slope angle. Under such conditions, the deposition thickness relative to the channel bed increases in the upstream direction. The deposition thickness at the first barrier can be expressed as follows:

$$H_{\mathrm{dh}} = H_{\mathrm{B2}} + L_{\mathrm{s}}\tan(\varphi - \theta) \tag{14}$$

Based on eq. (14), the deposition thickness will be always larger than the basal clearance height if $H_{\mathrm{c}} < H_{\mathrm{B2}}$. When $H_{\mathrm{c}} \geq H_{\mathrm{B2}}$, the maximum spacing to prevent blockage can be obtained by assuming $H_{\mathrm{dh}} = H_{\mathrm{c}}$:

$$L_{\mathrm{cs}} = \frac{H_{\mathrm{c}} - H_{\mathrm{B2}}}{\tan(\varphi - \theta)} \tag{15}$$

The clearance will not be jammed by the deposition if barrier spacing is smaller than L_{cs}.

Once the basal clearance is blocked by the accumulated debris from the second barrier, the interaction between subsequent flow and barriers can also be changed. Overflow from the first barrier lands directly into the deposited material, resulting in reduction of landing velocity (Kwan et al. 2015). As the landed flow propagating to downstream, the interaction between the flow and the newly deposited bed material may alter the flow mobility and consequently the impact forces on the second barrier. Mangeney et al. (2010) observed in their experiments that the erosion process of dry granular flows increased the flow mobility by up to 40% when slope was close to the angle of repose of the granular material. This implies that although the deposition may attenuate the landing velocity, the erosion process may also result in a larger impact velocity against the second barrier and therefore a larger landing distance downstream the second barrier. Thus, a larger barrier spacing between the second and third barriers may be required to ensure the barrier spacing is larger than the landing distance so that the flow energy can be attenuated (Ng et al. 2019).

In this section, the blockage of clearance is assessed based on the deposition thickness relative to the basal clearance. This method of assessment is necessary only for $H_{\mathrm{c}} \geq 3.0D$, where D is the particle size. For flow with much coarser particles, a stable arching can form by the particles when $H_{\mathrm{c}} \leq 1.5D$ and jam the basal clearance as observed by Choi et al. (2020).

Flow depth of basal discharge and landed flow

After the flow impacted the first barrier, flow discharged through the basal clearance or overflow on top of the barrier. The flow depth and velocity when propagating to downstream are essential for estimating the impact force on the second barrier. Figure 8 shows a comparison of the measured flow depth for different basal clearances after flow impacting the first barrier. Flow depths for only basal discharge (Fig. 8*a*) and combined overflow and basal discharge (Fig. 8*b*) are compared. The peak flow depths before flow impacting the second barrier were measured by the two ultrasonic sensors (Fig. 3) that were installed 300 mm ($L = 6h_0$) and 1100 mm ($L = 23h_0$) away from the first barrier. The locations of the ultrasonic sensors were determined based on the landing distance of the flow. When flow was about to land on the flume (no basal discharge) or the basal discharge, the distance between the frontal edge of the flow (Fig. 5*c*) and the barrier is obtained from the high-speed images as the landing distance. With an increase of basal clearance H_c from 0 to $0.8h_0$, overflow velocity was attenuated, resulting in a decreasing landing distance from $4.7h_0$ to $3.8h_0$. The average landing distance was $4.2h_0$ with a standard deviation of $0.4h_0$. Therefore, the measured flow depths by the two ultrasonic sensors at $L = 6h_0$ and $L = 23h_0$ can be representative for flow depths that were near and far from the landing location, respectively.

As the basal clearance increases, the flow depth of basal discharge (Fig. 8*a*) increases because the larger clearance enabled more particles to be discharged. When the flow propagates from a distance of $L = 6h_0$ to $L = 23h_0$ away from the first barrier, the flow depth decreases by up to 30%. The flow depth for only basal discharge is consistently smaller than the basal clearance height. Therefore, assuming the discharge flow depth as basal clearance height (ξ = 1.0) as reported by Choi et al. (2020) can provide an upper bound discharge depth to estimate the impact force of basal discharge. Moreover, the reduction factor of basal discharge depth ξ equals to 0.8 and 0.6 can well capture the discharge depth using eq. (6) at $L = 6h_0$ and $L = 23h_0$,

respectively, providing a design basis of selecting ξ based on the transportation distances.

When overflow occurs on the first barrier (Fig. 8*b*), flow depth at $L = 6h_0$ decreases by up to 23% when H_c/h_0 increases from 0.0 to 0.8 after landing. Since the maximum flow depth for barrier with overflow appears when there is no basal clearance, the decrease of the flow depth may mainly result from the reduction of overflow by basal discharge. The flow depth after landing exceeds the flow depth impacting on the first barrier by around 10% when H_c/h_0 ranges from 0.0 to 0.2 and $L = 6h_0$. This implies that the assuming the same flow depth impacting on the second barrier as the first barrier (Ng et al. 2019) may not be conservative if the second barrier is near the landing location. As the flow propagating to downstream at $L = 23h_0$, the flow thins by up to 57% for combined overflow and basal discharge. The flow depth can be more efficiently thinned when there is overflow compared with only basal discharge. This suggests a larger barrier spacing is more effective to reduce the impact flow depth when there are both overflow and basal discharge rather than only basal discharge.

Noted that the bulk density of the flow is also important for characterising the flow depth, flow velocity and impact force on barriers. In this study, the flow density is assumed as a constant of 1620 kg/m^3, which is the measured bulk density in the storage container. During the flow process, the dilation of the granular material can reduce the bulk density of the flow. The bulk density of the flow can be expressed as $\rho=v_s\rho_p$, where ρ_p was measured as 2650 kg/m^3. Therefore, the volumetric solid fraction of the flow material in the container was v_s=0.61, which is similar to the volumetric solid fraction of 0.60 for dry granular flows reported by other studies (Denlinger and Iverson 2001; Faug 2015). The similar density implies that assuming the flow density before impacting the first barrier is same as the initial density is reasonable (Savage and Hutter 1991; Pudasaini and Hutter 2007). This assumption is also applicable to dense granular flows with uniform glass beads as reported by Job et al. (2006). During the flow landing, the impact of the overflow on the landed flow as shown in Fig. 5*d* may lead the flow

at the landing location to be denser than the flow further downstream. However, the solid fraction of the flow cannot exceed 0.64, which is the maximum solid fraction that can be obtained by pouring monodisperse flow based on random close packing phenomenon (Onoda and Liniger 1990; Song et al. 2008). This implies that the landing of idealised monodisperse flow may increase the flow density before impacting the second barrier by up to 5% compared with the flow impacting on the first barrier. This also indicates that assuming a constant density is reasonable for monodisperse flow with spherical particles. However, for flows with non-uniform particles, the increased flow bulk density resulted by landing may be more significant and increase the impact force on the second barrier if the barrier is near the landing location. The changes of the flow density can be quantified using the constitutive equation proposed by Pouliquen et al. (2006) by characterising the inertial number of the flow.

Flow velocity of basal discharge and landed flow

Figure 9 shows a comparison of the measured flow velocity for different basal clearances after flow impacting the first barrier. Flow velocities were measured at the same locations as the ultrasonic sensors by using the two high-speed cameras (Fig. 3) following a same approach as measuring the frontal velocity at the first barrier. The initial discharge is mainly from the tapered thin flow front (Fig. 5*a*) that freely passes through the basal clearance and dominates the frontal velocity of the basal discharge. The frontal velocity of the basal discharge at $L = 23h_0$ is compared with proposed eq. (5). To evaluate the effects of basal clearance on the flow velocity, flow velocities for only basal discharge (Fig. 9*a*) were measured at the moment just before landing (Fig. 5*c*). When there is overflow, flow velocities after landing (Fig. 9*b*) were measured when the front of the landing flow propagated to the locations of ultrasonic sensors at $L = 6h_0$ and $L = 23h_0$. The discharge velocity is normalised by the impact velocity for the first barrier to indicate the effectiveness of basal clearance on attenuating the discharge velocity.

In contrast, the flow velocity after landing is normalised by the measured velocity just before landing (Fig. 5*c*). The normalised landing velocity indicates the landing factor C_r as expressed in eq. (3).

The measured frontal velocity of the basal discharge (Fig. 9*a*) increases by about 20% when H_c/h_0 increases from 0.2 to 0.4 and maintains similar when the basal clearance further increases. This indicates that a smaller basal clearance ($H_c = 0.2h_0$) can resist the frontal velocity of the basal discharge. For a larger basal clearance ($H_c \geq 0.4h_0$), the frontal velocity of the basal discharge is less resisted by the first barrier and can be estimated using the proposed eq. (5). Following the front of the basal discharge, the subsequent flow velocity of basal discharge increases with basal clearance by up to 66% when $L = 6h_0$. A basal clearance can effectively reduce the subsequent discharge velocity by up to 70% compared with the initial impact velocity on the first barrier, indicating the basal clearance is effective in regulating the flow discharge. When $L = 23h_0$, the flow accelerates by up to 157% and remains slower than the frontal discharge velocity.

When overflow occurs, flow velocity (Fig. 9*b*) at $L = 6h_0$ is near-constant when H_c/h_0 increases from 0.0 to 0.4 with a landing factor C_r close to 0.7 which has been recommended by Kwan et al. (2015) for rigid bed. As the normalised basal clearance H_c/h_0 increases to 0.8, the normalised landing velocity decreases by 34% with a minimum landing factor C_r of about 0.4. The decreased landing factor C_r indicates that the basal discharge is more effective in attenuating the landing velocity compared with a rigid bed when $H_c \geq 0.6h_0$. As observed in Figs. 5*c* and 5*d*, the basal discharge with a lower velocity than landing flow provides resistance to the flow after landing, resulting in attenuation of flow kinetic energy and reduction in landing factor C_r. However, this landing factor does not decrease when $H_c/h_0 \leq 0.4$, which may attribute to the less amount of the basal discharge has negligible effect on resisting the landing flow. When flow propagates to $L = 23h_0$, the flow accelerates by up to 93% for landed flow. The

substantial flow acceleration far from the landing location for overflow and basal discharge implies that the flow acceleration may also be an important consideration for designing the subsequent barriers with larger barrier spacing.

Flow velocities after landing calculated by the proposed eq. (9) are compared with the measured velocities. In eq. (9), the v_{Hc} is extracted from Fig. 4 as the flow velocity when flow depth equals to basal clearance height. Landing reduction factor C_r = 0.7 that has been recommended by Kwan et al. (2015) is adopted. By comparing with the measured landing velocity at $L = 6h_0$, the proposed eq. (9) overestimates the landing velocity by up to about 100%. The overestimation is mainly due to eq. (9) neglects the energy dissipation caused by the basal discharge and collisions among particles during the run-up process and adopts a conservative landing factor. Therefore, larger discrepancies appear when H_c/h_0 increases to 0.6 and 0.8. When $L = 23h_0$, the acceleration of the flow results in a close match of measured and calculated velocity after landing. It is expected that eq. (9) may underestimate the flow velocity if the flow propagates to further downstream due to the neglect of flow acceleration. Nevertheless, considering the flow thinning during the propagation (Fig. 8*b*), eq. (9) may serve as a reasonable first approximation to estimate the impact force of overflow.

Measured impact force on the second barrier

Figure 10 shows the typical time histories of normalised impact force on the second barrier with normalised basal clearances of 0.4 (Fig. 10*a*) and 0.8 (Fig. 10*b*) beneath the first barrier. The impact force is normalised by the theoretical impact force of the first barrier calculated by hydrodynamic equation eq. (4) with α = 1.0, indicating the impact force ratio between the two barriers.

When the first barrier has a basal clearance of $H_c/h_0 = 0.4$ (Fig. 10*a*), the impact force from the basal discharge of the tall barrier ($H_{B1}/h_0 = 10$) first increases to a peak and then

decreases to reach a static force. The increase of the impact force was mainly resulted by the freely passed tapered thin front as observed in Fig. 5*a*. Once the flow was resisted by the first barrier, the dynamic load on the second barrier from the basal discharge was attenuated and the total impact force would be dominated by the static force. In contrast, for the short first barrier ($H_{B1}/h_0 = 2$) that allows both basal discharge and overflow, the impact force on the second barrier increases with a similar loading process to the tall barrier ($H_{B1}/h_0 = 10$) before $t = 1.00$ s. Then, under the impact of the overflow from the first barrier, the impact force increases to the peak and decreases by about 10% to static. For a much larger basal clearance of $H_c/h_0 = 0.8$ (Fig. 10*b*) beneath the first barrier, the impact force by the basal discharge of the tall barrier ($H_{B1}/h_0 = 10$) substantially increases compared with the force as shown in Fig. 10*a*. This is because more flow is discharged through the enlarged basal clearance. The impact forces on the second barrier for both the short ($H_{B1}/h_0 = 2$) and tall ($H_{B1}/h_0 = 10$) barriers are also similar within $t = 1.00$ s. However, as to the short barrier, after the impact of the basal discharge, the subsequent impact from the overflow only slightly increases the total impact load and is less than the impact force exerted by the basal discharge. This is because the overflow is more significantly reduced by the larger basal clearance. The larger amount of deposition from the basal discharge also provided a much thicker cushioning layer and attenuated the impact force from the overflow more efficiently.

The impact time of the basal discharge can be used to evaluate the proposed eq. (5) of estimating the impact velocity of basal discharge. For the first barrier that has a basal clearance of $H_c/h_0 = 0.4$ (Fig. 10*a*) and $H_c/h_0 = 0.8$ (Fig. 10*b*), the basal discharge reaches the second barrier at $t = 0.40$ s and $t = 0.34$ s, respectively. Time $t = 0.00$ s denotes the moment that flow just impacts on the first barrier. By assuming that the flow impacts on the barrier when flow depth reaches the basal clearance height, it can be inferred from Fig. 4 that the flow impacts on the barrier 0.15 s after flow reaching the first barrier location for $H_c/h_0 = 0.4$ and 0.27 s for

H_c/h_0 = 0.8. Therefore, the transportation time of basal discharge between the two barriers for H_c/h_0 = 0.4 is 0.55 s and for H_c/h_0 = 0.8 is 0.61 s. The average basal discharge velocities between the two barriers for H_c/h_0 equals to 0.4 and 0.8 are 2.5 m/s and 2.3 m/s, respectively, which are close to the average basal discharge velocity of 2.4 m/s estimated by eq. (5). This suggests that it is reasonable to estimate the frontal basal discharge velocity using eq. (5). The proposed methods using eqs. (7) and (10) to estimate the impact forces from basal discharge and overflow are also compared with the measured impact forces and show reasonable predictions. The calculated larger impact force from basal discharge and overflow serves as a reasonably conservative prediction of the peak impact force on the second barrier, suggesting the suitability of using eq. (11) to predict the impact force from combined basal discharge and overflow. Details of the proposed equations are discussed in the following section.

Evaluation of the newly proposed equations

Figure 11 shows a comparison of the measured and calculated peak impact forces on the second barrier with different first barrier heights and varying basal clearances beneath the first barrier. The first barrier with a height of H_{B1}/h_0 = 2 represents a short barrier where both basal discharge and overflow can occur, while H_{B1}/h_0 = 10 represents a tall barrier where only basal discharge can occur. When there is no overflow on the first barrier, the impact force on the second barrier is entirely due to the basal discharge passing underneath the first barrier. Without overflow, the impact force on the second barrier increases with increasing basal clearance. On the contrary, for the shorter first barrier that allows overflow, the impact force on the second barrier decreases when H_c/h_0 ranges from 0.0 to 0.6 and reaches a minimum impact force when H_c/h_0 = 0.6. As discussed in the measured time histories of the impact force on the second barrier (Fig. 10), the decrease of impact force is mainly attributed to the reduced overflow and the cushioning effect from the deposition of the basal discharge. When H_c/h_0 = 0.8, the impact

force on the second barrier increases since the impact is dominated by basal discharge. This implies that the impact force on the second barrier for $H_c/h_0 \leq 0.6$ and $H_c/h_0 > 0.6$ can be estimated from the impact forces of overflow and basal discharge, respectively.

The performance of the newly proposed equations to estimate the impact force on the second barrier is evaluated. Details of input parameters and the procedures of using the newly proposed equations to estimate the impact force on the second barrier are introduced in Appendix A. Proposed eq. (7) can capture the trend and reasonably predict the impact force on the second barrier by basal discharge. For the tests where both overflow and basal discharge occur at the first barrier, the impact force on the second barrier calculated using eq. (10) is larger than eq. (7) when $H_c/h_0 \leq 0.4$ and slightly lower than eq. (7) by 5% when H_c/h_0 equals to 0.6. When H_c/h_0 equals to 0.8, the impact force calculated by eq. (7) is about 50% higher than that calculated by eq. (10). This is because the larger basal clearance results in a dominant impact force by basal discharge (Fig. 10*b*) when $H_c/h_0 = 0.8$. By adopting the larger impact force calculated from eqs. (7) and (10), eq. (11) can reasonably estimate the peak impact force from combined basal discharge and overflow. More importantly, eq. (11) captures the minimum impact force, indicating that there is a potential of using eq. (11) to optimise the design of multiple barriers with an optimal basal clearance.

The analytical equations for estimating the impact forces of basal discharge and overflow on the second barrier from this study have only been evaluated for the dry granular flow with a Froude number of 3. Although this value lies within the typical range of Froude numbers in the field (Hübl et al. 2009), it still warrants further evaluation of the analytical solutions for flows with much lower (e.g. subcritical flow with $Fr < 1$) or higher ($Fr > 5$) Froude numbers. Faug (2021) compared the impact dynamics of slow and fast granular flows and proposed two different analytical solutions to estimate the impact forces of slow ($Fr < 1$) and fast ($Fr > 5$) granular flows. The necessity for characterising the impact dynamics based

on slow and fast flows is because of the prevailing impact mechanism. More specifically, a pile-up process was observed for subcritical flows with $Fr < 1$ and a granular jump (run-up) was observed for supercritical flows with $Fr > 5$. In this study, the impact mechanism resembles a pile-up process (Fig. 5). It is expected that flows with a pile-up process may have similar overflow and landing dynamics because they are consistent with the assumptions made in eqs. (1) and (2) used to estimate the landing distance and landing velocity. For supercritical flows with $Fr > 5$, the granular jump may lead to flow material launching from the first barrier at different angles compared with a pile-up process. The changing in launching angle may result in different landing distance and velocity. Further study on the effects of a granular jump on the landing dynamics of granular flow is still warranted. Once the flow velocity and depth of landed flow and basal discharge can be reasonably estimated and implemented into the equations proposed by Faug (2021), the impact force on the second barrier for flows with a wide range of Froude numbers can be predicted.

The barriers in this study were oriented orthogonally to the flume base. In the field, barriers may orient either orthogonally or vertically with respect to the channel bed (Rudolf-Miklau et al. 2015; Wendeler 2016). Different barrier orientations may affect not only the impact force on the barrier but also the basal discharge. For the impact force, the orthogonal barrier may have larger impact force compared with vertical barriers following the design guideline by Kwan (2012) due to the perpendicular impact direction of the flow against the barrier. For the basal discharge, experimental results from Sheldon and Durian (2010) indicate that the discharge of granular flow in an orthogonal barrier is larger than vertical barrier with a same basal clearance. Therefore, the results of impact force of basal discharge obtained from orthogonal barriers may provide conservative estimations of the impact force on the second barrier when barriers are oriented vertically. Although the less basal discharge in a vertical barrier may lead to larger overflow volume, the proposed eq. (10) to estimate the overflow

impact force have neglected the effects of reduced overflow volume resulted by basal discharge. Therefore, eq. (10) can still serve to estimate the overflow impact force for vertical barriers.

Conclusions

A series of 5-m-long flume tests have been conducted to investigate the impact dynamics of dry granular flow on dual rigid barriers with varying basal clearances beneath the first barrier. The dry granular flow was composed of 3-mm glass beads with a Froude number of $Fr = 3$ at the first barrier location. Furthermore, a new approach based on the hydrodynamic equation, is proposed to estimate the impact force exerted by basal discharge and overflow. The approach has been evaluated using the physical experiments for different ratios between basal clearance H_c and flow depth h_0. Key conclusions from this study may be drawn as follows:

a) The new approach for estimating the impact force exerted by the basal discharge and overflow from the first barrier on the second barrier provides reasonable conservative results for a wide range of basal clearances ($0.2 \leq H_c/h_0 \leq 0.8$). The new equations provide a basis for optimising the resisting forces for multiple barrier systems with basal clearances.

b) The basal clearance of the first barrier (barrier height $H_{B1} = 2h_0$) can regulate the impact force exerted on the second barrier by dissipating the kinetic energy of landing flow and apportioning the load contributions from basal discharge and overflow. Flow velocity reduced by up to 60% after flow landing on the basal discharge, while flow velocity reduced about 30% after flow landing on a rigid channel bed. The basal discharge governs the impact force when $H_c/h_0 \geq 0.8$. Overflow governs the impact force when $H_c/h_0 \leq 0.6$. These two criteria can be used to optimise the design height and size of basal clearance.

c) For dual barriers, where the second barrier is a closed barrier, the spacing between barriers can be positioned to prevent pileup from the second barrier from jamming the basal clearance of the first barrier. A new criterion based on the retained geometric profile behind the second barrier is proposed to remedy this problem. This criterion can be used to minimise the maintenance required for the first barrier.

Results from this study are based on an idealised dry granular flow. For two-phase debris flows, the interaction between the fluid and solid phases can reduce the contact stress of granular assembly (McArdell et al. 2007; Iverson et al. 2010; Ng et al. 2021) and facilitate the basal discharge. Therefore, the impact force of basal discharge on the second barrier is expected to be larger. The proposed analytical method for estimating the impact force of the basal discharge on the second barrier adopts the hydrodynamic approach and assumes energy conservation during impact. Therefore, this proposed method may still be suitable for estimating the impact force of basal discharge for two-phase debris flow, where the reduced contact stress within the granular assembly leads to less frictional energy dissipation compared with dry granular flow. In contrast, the proposed analytical equations for estimating overflow and landing dynamics may not be appropriate for debris flows. Although the larger basal discharge of debris flow may reduce the overflow volume, the jet-like run-up of debris flow upon impact (Ng et al. 2021) may also cause larger overflow distance compared with dry granular flows. The effects of basal discharge on the overflow distance and landing velocity of debris flow still require further study for the design of multiple barriers with basal clearance against debris flows.

Acknowledgements

The work described in this paper was supported by a grant from the Research Grants Council

of the Hong Kong Special Administrative Region, China (Project Nos. AoE/E-603/18, T22-603/15N, 16212618, 16209717 and 27205320). The authors are grateful for the financial sponsorship from the National Natural Science Foundation of China (51709052).

References

Arattano, M., Deganutti, A.M., and Marchi, L. 1997. Debris flow monitoring activities in an instrumented watershed on the Italian Alps. *In* Proceedings of the 1st ASCE International Conference on Debris-Flow Hazards Mitigation: Mechanics, Prediction & Assessment, San Francisco, California, USA, pp. 506–515.

Armanini, A., Larcher, M., and Odorizzi, M. 2011. Dynamic impact of a debris flow front against a vertical wall. *In* Proceedings of the 5th International Conference on Debris-Flow Hazards Mitigation: Mechanics, Prediction and Assessment, Padua, Italy, pp. 1041–1049.

Ashwood, W., and Hungr, O. 2016. Estimating total resisting force in flexible barrier impacted by a granular avalanche using physical and numerical modeling. Canadian Geotechnical Journal, **53**(10): 1700–1717. doi:10.1139/cgj-2015-0481.

Chiari, M., Moser, M., Trojer, M., and Hübl, J. 2016. Physical scale experiments on torrential filter structures. *In* EGU General Assembly Conference Abstracts (Vol. 18, p. 6406), Vienna, Austria.

Choi, C.E., Ng, C.W.W., Goodwin, G.R., Liu, L.H.D., and Cheung, W.W. 2016. Flume investigation of the influence of rigid barrier deflector angle on dry granular overflow mechanisms. Canadian Geotechnical Journal, **53**(10): 1751–1759. doi: 10.1139/cgj-2015-0248.

Choi, C.E., Cui, Y., Liu, L.H.D., Ng, C.W.W., and Lourenço, S.D.N. 2017. Impact mechanisms of granular flow against curved barriers. Géotechnique Letters, **7**(4): 330–338. doi:10.1680/jgele.17.00068.

Choi, C.E., Ng, C.W.W., Liu, H., and Wang, Y. 2020. Interaction between dry granular flow and rigid barrier with basal clearance: Analytical and physical modelling. Canadian Geotechnical Journal, **57**(2): 236–245. doi:10.1139/cgj-2018-0622.

Denlinger, R.P., and Iverson, R.M. 2001. Flow of variably fluidized granular masses across three-dimensional terrain: 2. Numerical predictions and experimental tests. Journal of Geophysical Research: Solid Earth, **106**(B1): 553–566. doi:10.1029/2000JB900330.

Faug, T. 2015. Macroscopic force experienced by extended objects in granular flows over a very broad Froude-number range. Eur. Phys. J. E, **38**: 34. doi:10.1140/epje/i2015-15034-3.

Faug, T. 2021. Impact force of granular flows on walls normal to the bottom: Slow versus fast impact dynamics. Canadian Geotechnical Journal, **58**(1): 114–124. doi:10.1139/cgj-2019-0399.

Faug, T., Caccamo, P., and Chanut, B. 2012. A scaling law for impact force of a granular avalanche flowing past a wall, Geophysical Research Letters, **39**, L23401, doi:10.1029/2012GL054112.

Glassey, T. 2013. Hydrology and check dams analysis in the debris flow context of Illgraben torrent. MAS practical research project, Swiss Federal Institute of Technology, Zurich, Switzerland.

Hákonardóttir, K.M., Hogg, A.J., Batey, J., and Wood, A.W. 2003. Flying avalanches. Geophysical Research Letters, **30**(23): 1–4. doi:10.1029/2003GL018172.

Hübl, J., Suda, J., Proske, D., Kaitna, R., and Scheidl, C. 2009. Debris flow impact estimation. *In* Proceedings of the 11th International Symposium on Water Management and Hydraulic Engineering, Ohrid, Macedonia, pp. 1–5.

Iverson, R.M. 2015. Scaling and design of landslide and debris-flow experiments. Geomorphology, **244**, 9–20. doi:10.1016/j.geomorph.2015.02.033.

Iverson, R.M., Logan, M., and Denlinger, R.P. 2004. Granular avalanches across irregular three-dimensional terrain: 2. Experimental tests. Journal of Geophysical Research: Earth Surface, **109**(F1): 1–16. doi:10.1029/2003jf000084.

Iverson, R.M., Logan, M., LaHusen, R.G., and Berti, M. 2010. The perfect debris flow? Aggregated results from 28 large-scale experiments. Journal of Geophysical Research, **115**(F3), F03005. doi:10.1029/2009jf001514.

Jop, P., Forterre, Y., and Pouliquen, O. 2006. A constitutive law for dense granular flows. Nature, **441**(7094): 727–730. doi:10.1038/nature04801.

Kwan, J.S.H. 2012. Supplementary technical guidance on design of rigid debris resisting barriers. Technical Note No. TN 2/2012. Geotechnical Engineering Office, Civil Engineering and Development Department, The HKSAR Government.

Kwan, J.S.H., Koo, R.C.H., and Ng, C.W.W. 2015. Landslide mobility analysis for design of multiple debris-resisting barriers. Canadian Geotechnical Journal, **52**(9): 1345–1359. doi:10.1139/cgj-2014-0152.

Kwan, J.S.H., and Koo, R.C.H. 2015. Preliminary back analysis of open hillside landslide impacting on a flexible rockfall barrier at Jordan Valley. Report No. 308. Geotechnical Engineering Office, Civil Engineering and Development Department, The HKSAR Government.

Mangeney, A., Roche, O., Hungr, O., Mangold, N., Faccanoni, G., and Lucas, A. 2010. Erosion and mobility in granular collapse over sloping beds. Journal of Geophysical Research: Earth Surface, **115**(3): 1–21. doi:10.1029/2009JF001462.

McArdell, B.W., Bartelt, P., and Kowalski, J. 2007. Field observations of basal forces and fluid pore pressure in a debris flow. Geophysical Research Letters, **34**(7). doi:10.1029/2006GL029183.

Morstabilini, C., and Deana, M.L. 2019. Laboratory tests of an innovative check dam. *In* Debris-Flow Hazards Mitigation: Mechanics, Monitoring, Modeling, and Assessment - Proceedings of the 7th International Conference on Debris-Flow Hazards Mitigation, Colorado, USA, pp. 1004–1011.

Morstabilini, C., Boschini, I., Zambrini, F., Menduni, G., Deana, M.L., and Zorzi, N. 2019. Application of an innovative, low-maintenance weir to protect against debris flows and floods in Ottone, Italy. *In* Debris-Flow Hazards Mitigation: Mechanics, Monitoring, Modeling, and Assessment - Proceedings of the 7th International Conference on Debris-Flow Hazards Mitigation, Colorado, USA, pp. 996–1003.

Nagl, G., Hübl, J., and Chiari, M. 2016. Experimental testing of impact force on rigid and flexible barriers - A comparison. *In* EGU General Assembly Conference Abstracts (Vol. 18, p. 6991), Vienna, Austria.

Ng, C.W.W., Choi, C.E., and Law, R.P.H. 2013. Longitudinal spreading of granular flow in trapezoidal channels. Geomorphology, **194**: 84–93. doi:10.1016/j.geomorph.2013.04.016.

Ng, C.W.W., Choi, C.E., Goodwin, G.R., and Cheung, W.W. 2017*a*. Interaction between dry granular flow and deflectors. Landslides, **14**(4). doi:10.1007/s10346-016-0794-3.

Ng, C.W.W., Choi, C.E., Liu, L.H.D., Wang, Y., Song, D., and Yang, N. 2017*b*. Influence of particle size on the mechanism of dry granular run-up on a rigid barrier. Géotechnique Letters, **7**(1): 79–89. doi:10.1680/jgele.16.00159.

Ng, C.W.W., Choi, C.E., Koo, R.C.H., Goodwin, G.R., Song, D., and Kwan, J.S.H. 2018. Dry granular flow interaction with dual-barrier systems. Géotechnique, **68**(5): 386–399. doi: 10.1680/jgeot.16.P.273.

Ng, C.W.W., Choi, C.E., Majeed, U., Poudyal, S., and De Silva, W.A.R.K. 2019. Fundamental framework to design multiple rigid barriers for resisting debris flows. *In* Proceedings of

the 16th Asian Regional Conference on Soil Mechanics and Geotechnical Engineering, Taipei, Taiwan, China, pp. 1–11.

Ng, C.W.W., Choi, C.E., Liu, H., Poudyal, S. and Kwan, J.S.H. 2021. Design recommendations for single and dual debris flow barriers with and without basal clearance. *In* Understanding and Reducing Landslide Disaster Risk. WLF 2020. ICL Contribution to Landslide Disaster Risk Reduction. Springer, Cham. doi:10.1007/978-3-030-60196-6_2.

Onoda, G.Y., and Liniger, E.G. 1990. Random loose packings of uniform spheres and the dilatancy onset. Physical Review Letters, **64**(22), 2727. doi:10.1103/PhysRevLett.64.2727.

Piton, G., and Recking, A. 2015. Design of sediment traps with open check dams. I: Hydraulic and deposition processes. Journal of Hydraulic Engineering, **142**(2), 04015045. doi:10.1061/(ASCE)HY.1943-7900.0001048.

Pouliquen, O., Cassar, C., Jop, P., Forterre, Y., and Nicolas, M. 2006. Flow of dense granular material: towards simple constitutive laws. Journal of Statistical Mechanics: Theory and Experiment, **2006**(07), P07020. doi:10.1088/1742-5468/2006/07/P07020.

Pudasaini, S. P., and Hutter, K. 2007. Avalanche dynamics: dynamics of rapid flows of dense granular avalanches. Springer Science & Business Media.

Rudolf-Miklau, F., Sauermoser, S., and Mears, A. I. 2015. The technical avalanche protection handbook. Berlin: Ernst & Sohn.

Savage, S.B., and Hutter, K. 1991. The dynamics of avalanches of granular materials from initiation to runout. Part I: Analysis. Acta Mechanica, **86**(1): 201–223. doi:10.1007/BF01175958.

Sheldon, H. G., and Durian, D. J. 2010. Granular discharge and clogging for tilted hoppers. Granular Matter, **12**(6): 579–585. doi:10.1007/s10035-010-0198-3.

Song, C., Wang, P., and Makse, H. A. 2008. A phase diagram for jammed matter. Nature, **453**(7195): 629–632. doi:10.1038/nature06981.

Sze, E., and Lam, H. 2017. Some suggested detailing of flexible barriers traversing a stream course for drainage purposes. Technical Note No. TN 3/2017. Geotechnical Engineering Office, Civil Engineering and Development Department, The HKSAR Government.

Thielicke, W. 2014. The Flapping Flight of Birds - Analysis and Application. PhD Thesis, University of Groningen, Groningen, Netherlands.

Thielicke, W., and Stamhuis, E.J. 2014. PIVlab – Towards User-friendly, Affordable and Accurate Digital Particle Image Velocimetry in MATLAB. Journal of Open Research Software, **2**. doi:10.5334/jors.bl.

VanDine, D.F. 1996. Debris Flow Control Structures for Forest Engineering. Ministry of Forests, British Columbia, Canada, 68 p.

Volkwein, A. 2014. Flexible debris flow barriers: Design and application. WSL Berichte, 18. Birmensdorf, Swiss Federal Institute for Forest, Snow and Landscape Research WSL. 29 p.

Wendeler, C. 2016. Debris-flow protection systems for mountain torrents. WSL Berichte. Swiss Federal Institute for Forest, Snow and Landscape Research WSL.

Wendeler, C., Volkwein, A., Roth, A., Herzog, B., Hahlen, N., and Wenger, M. 2008. Hazard prevention using flexible multi-level debris flow barrier. In *Interpraevent* (Vol. 1, pp. 547–554).

Wendeler, C., Volkwein, A., McArdell, B.W., and Bartelt, P. 2019. Load model for designing flexible steel barriers for debris flow mitigation. Canadian Geotechnical Journal, **56**(6): 893–910. doi:10.1139/cgj-2016-0157.

WSL. 2008. Integral risk management of extremely rapid mass movements. Swiss Federal Institute for Snow and Avalanche Research. Available from http://irasmos.slf.ch/ [cited

24 September 2020].

Yang, Q., Cai, F., Ugai, K., Yamada, M., Su, Z., Ahmed, A., Huang, R., and Xu, Q. 2011. Some factors affecting mass-front velocity ofrapid dry granular flows in a large flume. Engineering Geology, **122**: 249–260. doi:10.1016/j.enggeo.2011. 06.006.

List of symbols

C_r landing factor

D particle size (m)

F impact force of flow on barrier (N)

F_d impact force of basal discharge (N)

F_L impact force of overflow (N)

Fr Froude number

F_T impact force from combined basal discharge and overflow (N)

$\boldsymbol{g}$ gravitational acceleration (m/s^2)

h_0 maximum flow depth at the first barrier (m)

H_1 height from the top of the first barrier to the channel bed (m)

H_{B1} first barrier height (m)

H_{B2} second barrier height (m)

H_c basal clearance height (m)

h_d flow depth of basal discharge (m)

H_{dh} deposition height at the first barrier location (m)

L transportation distance away from the first barrier (m)

L_{cs} critical barrier spacing to prevent the blockage of basal clearance (m)

L_s barrier spacing (m)

t time (s)

v flow velocity (m/s)

v_1 frontal velocity at first barrier (m/s)

v_{Hc} impact velocity on barrier when flow depth reaches basal clearance height (m/s)

v_i flow velocity after landing (m/s)

v_m overflow velocity (m/s)

v_r flow velocity just before landing (m/s)

v_s solid fraction of the flow

w flume width (m)

x_i overflow distance (m)

α hydrodynamic impact coefficient

θ slope angle (°)

ξ reduction factor of basal discharge depth

ρ flow density (kg/m^3)

ρ_p particle density (kg/m^3)

φ friction angle of flow-bed interface (°)

List of Table

List of Figures

APPENDIX A. Input parameters and procedures of using the newly proposed eqs. (7) and (11)

This section introduces the input parameters and procedures of using the newly proposed equations to estimate the impact force on the second barrier due to basal discharge and overflow from the first barrier. Moreover, international design recommendations associated with the parameter determination are also introduced. The parameters for the newly proposed equations are summarised in Table A1.

Determination of α, ξ, and C_r

A theoretical hydrodynamic impact coefficient $\alpha = 1.0$ is adopted by this study. Recent study by Ng et al. (2021) and an updated design guideline by GEO (2020) recommend $\alpha = 1.5$ for designing rigid barriers. The reduction factor of basal discharge depth $\xi = 0.6$ is adopted in this study based on the measured results as shown in Fig. 8a, where ξ decreases with increasing flow propagation distance from the first barrier. The ξ decreases from 0.8 to 0.6 when the flow propagation distance increases from $6h_0$ to $23h_0$ away from the first barrier. Landing factor $C_r = 0.7$, which has been recommended by Kwan et al. (2015) as a conservative value to estimate the landing velocity, is used in this study.

Determination of v_1, h_0, and v_{Hc}

The frontal flow velocity v_1 and maximum flow depth h_0 were measured using high-speed camera. For barriers with varying basal clearance heights, the flow starts to impact the barrier when the flow depth is equal to the basal clearance height. Therefore, the impact velocities v_{Hc} for barrier with different basal clearances were taken as the corresponding flow velocity when flow depth equals to basal clearance height from the measured time histories of flow depth and

velocity (Fig. 4).

In practice, the international design guidelines (Kwan 2012; ASI 2013; GEO 2020) recommend different debris mobility models to predict the hydrographs of flow depth and velocity at the barrier location to estimate the impact force. Hence, the hydrographs of flow depth and velocity obtained from the debris mobility analysis can serve to estimate the frontal velocity v_1, maximum flow depth h_0, and the impact velocity v_{Hc} for barrier with a basal clearance.

Determination of H_c, H_{B1}, and L_s

The basal clearance height H_c is varied from 0 to $0.8h_0$ to study the effects of basal clearance beneath the first barrier on the impact dynamics of second barrier. The first barrier with height H_{B1} equals to $2h_0$ and $10h_0$ has been selected to enable and prevent overflow, respectively. Barrier spacing of $L_s = 29h_0$ has been adopted to allow a relative far propagating distance for flow after landing so that the flow depth and flow velocity of the landed flow can be investigated.

In practice, basal clearance height H_c, first barrier height H_{B1}, and barrier spacing L_s are key design considerations that govern the retention volume and impact forces. The retention volume of the multiple barriers can be examined following the approach reported by VanDine (1996). For barriers with basal clearance, the jamming of the basal clearance should also be examined to determine the retention capacity of the barriers using eqs. (13) and (15) together with the proposed criterion proposed by Choi et al. (2020). Aside from reaching the design retention volume, the barrier spacing L_s should also be larger than the overflow distance estimated by eq. (1) to facilitate the energy dissipation during landing as suggested by Ng et al. (2021). The impact force on the first barrier with basal clearance can be estimated following the approach proposed by Choi et al. (2020). The impact forces of basal discharge and overflow

on the second barrier can be estimated using eqs. (7) and (11).

Impact force calculation

In this section, the test, where the barrier height is 100 mm and basal clearance height is 20 mm (test ID: B1C2), is taken for an example to illustrate the application of the newly proposed equations. First, the run-up height of the flow is estimated by the Froude number and the flow depth, h_0, of the flow using the momentum approach recommended by Kwan (2012) to determine the occurrence of overflow. The calculated run-up height is 0.24 m, which is larger than the total barrier height, suggesting that overflow can occur and the impact force on the second barrier should be examined by both basal discharge and overflow.

In order to obtain v_{Hc}, flow velocity when the flow depth equals to the basal clearance of first barrier is extracted from Fig. 4. Corresponding to basal clearance of 20 mm, the impact velocity v_{Hc} = 1.9 m/s.

Impact force of basal discharge

Flow velocity and depth of basal discharge before impacting on the second barrier are calculated using eqs. (5) and (6) and the results are given as follows:

$$v_{\mathrm{d}} = \sqrt{v_1^2 + 2L_{\mathrm{s}}g\,(\sin\theta - \tan\varphi\cos\theta)} = 2.8\ \mathrm{m/s}$$

$$h_{\mathrm{d}} = \xi H_{\mathrm{c}} = 0.012\ \mathrm{m}$$

Impact force of basal discharge is then obtained as follows:

$$F_{\mathrm{d}} = \alpha\rho v_{\mathrm{d}}^2 h_{\mathrm{d}} w = 30.5\ \mathrm{N}$$

Impact force of overflow

Overflow velocity and overflow distance are calculated using eqs. (8) and (1) as follows:

$$v_{\mathrm{m}} = \sqrt{v_{\mathrm{Hc}}^2 - 2gH_{\mathrm{B1}}(\cos\theta + \sin\theta\tan\varphi)} = 1.3\ \mathrm{m/s}$$

$$x_{\mathrm{i}} = \frac{v_{\mathrm{m}}^2}{g\cos\theta}\left[\tan\theta + \sqrt{\tan^2\theta + \frac{2gH_{\mathrm{B1}}}{v_{\mathrm{m}}^2\cos\theta}}\right] + H_{\mathrm{B1}}\tan\theta = 0.36\ \mathrm{m}$$

Velocity after landing is then estimated using eq. (9) as follows:

$$v_{\mathrm{i}} = C_{\mathrm{r}}\sqrt{v_{\mathrm{Hc}}^2 + 2g\sin\theta(x_{\mathrm{i}} - H_{\mathrm{B1}}\tan\varphi)} = 1.8\ \mathrm{m/s}$$

Impact force of overflow estimated by eq. (10) is given as follows:

$$F_{\mathrm{L}} = \ \alpha\rho h_0 w v_{\mathrm{i}}^2 = 48.3\ \mathrm{N}$$

Impact force from combined basal discharge and overflow

According to eq. (11), the impact force on the second barrier is finally obtained as follows:

$$F_{\mathrm{T}} = \ \max\left(F_{\mathrm{d}}, F_{\mathrm{L}}\right) = \max\left(30.5, 48.3\right) = 48.3\ \mathrm{N}$$

References

ASI. 2013. Protection works for torrent control – static and dynamic actions on structures. Austrian Standards Institute. ONR 24801:2013.

Choi, C.E., Ng, C.W.W., Liu, H., and Wang, Y. 2020. Interaction between dry granular flow and rigid barrier with basal clearance: Analytical and physical modelling. Canadian Geotechnical Journal, **57**(2): 236–245. doi:10.1139/cgj-2018-0622.

GEO. 2020. Enhanced technical guidance on design of rigid debris-resisting barriers. Technical Guidance Note No. 52. Geotechnical Engineering Office, Civil Engineering and Development Department, The HKSAR Government.

Kwan, J.S.H. 2012. Supplementary technical guidance on design of rigid debris resisting barriers. Technical Note No. TN 2/2012. Geotechnical Engineering Office, Civil Engineering and Development Department, The HKSAR Government.

Kwan, J. S. H., Koo, R. C. H., and Ng, C. W. W. 2015. Landslide mobility analysis for design of multiple debris-resisting barriers. Canadian Geotechnical Journal, **52**(9): 1345–1359.

doi:10.1139/cgj-2014-0152.

Ng, C.W.W., Choi, C.E., Majeed, U., Poudyal, S., and De Silva, W.A.R.K. 2019. Fundamental framework to design multiple rigid barriers for resisting debris flows. *In* Proceedings of the 16th Asian Regional Conference on Soil Mechanics and Geotechnical Engineering, Taipei, Taiwan, China, pp. 1–11.

Ng, C.W.W., Choi, C.E., Liu, H., Poudyal, S. and Kwan, J.S.H. 2021. Design recommendations for single and dual debris flow barriers with and without basal clearance. *In* Understanding and Reducing Landslide Disaster Risk. WLF 2020. ICL Contribution to Landslide Disaster Risk Reduction. Springer, Cham. doi:10.1007/978-3-030-60196-6_2.

Pudasaini, S. P., and Hutter, K. 2007. Avalanche dynamics: dynamics of rapid flows of dense granular avalanches. Springer Science & Business Media.

VanDine, D.F. 1996. Debris Flow Control Structures for Forest Engineering. Ministry of Forests, British Columbia, Canada, 68 p.

Table 1. Test programme.

Test ID	Height of first barrier, H_{B1} (mm)	Basal clearance height, H_c (mm)	H_{B1}/h_0	H_c/h_0
C	—	—	—	—
B1C0	100	0	2	0.0
B1C1	100	10	2	0.2
B1C2	100	20	2	0.4
B1C3	100	30	2	0.6
B1C4	100	40	2	0.8
B5C1	500	10	10	0.2
B5C2	500	20	10	0.4
B5C3	500	30	10	0.6
B5C4	500	40	10	0.8

Note: the flow depth h_0 was the maximum flow depth at the first barrier location obtained from the control test without installing any barrier.

Table A1. Summary of parameters for the newly proposed equations.

Parameter	Value (this study)	Method of determination (this study)	International design recommendation
Hydrodynamic impact coefficient, α	1.0	Theoretical value for rigid barrier	1.5 (GEO 2020; Ng et al. 2021)
Flow density, ρ (kg/m^3)	1620	Measured initial bulk density	1700 to 2000 for stony debris flow and 2000 to 2300 for muddy debris flow (ASI 2013)
Reduction factor of basal discharge depth, ξ	0.6	Measured (Fig. 8a)	—
Basal clearance height, H_c (m)	0 to 0.04	Varies from 0 to $0.8h_0$	—
Flow width, w (m)	0.2	Experiment setup	Topography or debris mobility analysis (Kwan 2012; ASI 2013)
Frontal velocity at first barrier, v_1 (m/s)	2.1	Measured	Debris mobility analysis (Kwan 2012; ASI 2013)
Barrier spacing, L_s (m)	1.4	Experiment setup	VanDine (1996)
Slope angle of the flume, θ (°)	25	Experiment setup	Topography (Kwan 2012)
Friction angle of flow-bed interface, φ (°)	18	Measured	Tilting test (Pudasaini and Hutter 2007)
Maximum flow depth, h_0 (m)	0.048	Measured	Debris mobility analysis (Kwan 2012; ASI 2013)
Landing factor (C_r)	0.7	Suggested by Kwan et al. (2015)	0.7 (Ng et al. 2019)
Impact velocity on the barrier when flow depth reaches basal clearance height (v_{Hc})	Varies	Measured from control test (Fig. 4)	Debris mobility analysis (Kwan 2012; ASI 2013)
Overflow distance (x_i)	Varies	Calculated by Eqs. (1) and (8)	Ng et al. (2019)

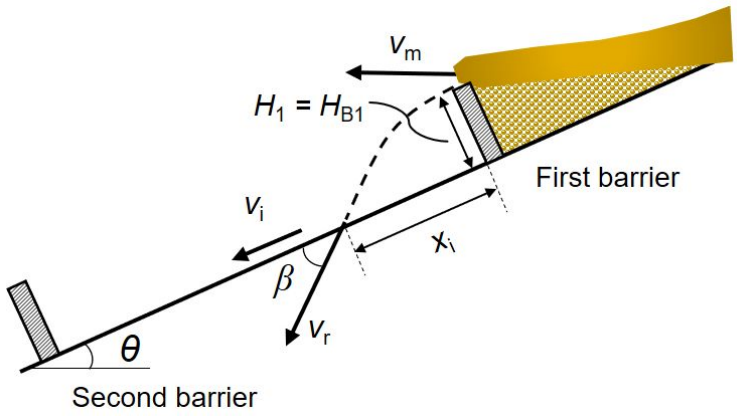

Fig. 1. Schematic of the interaction between flow and multiple rigid barriers without basal clearance (Kwan et al. 2015; Ng et al. 2019).

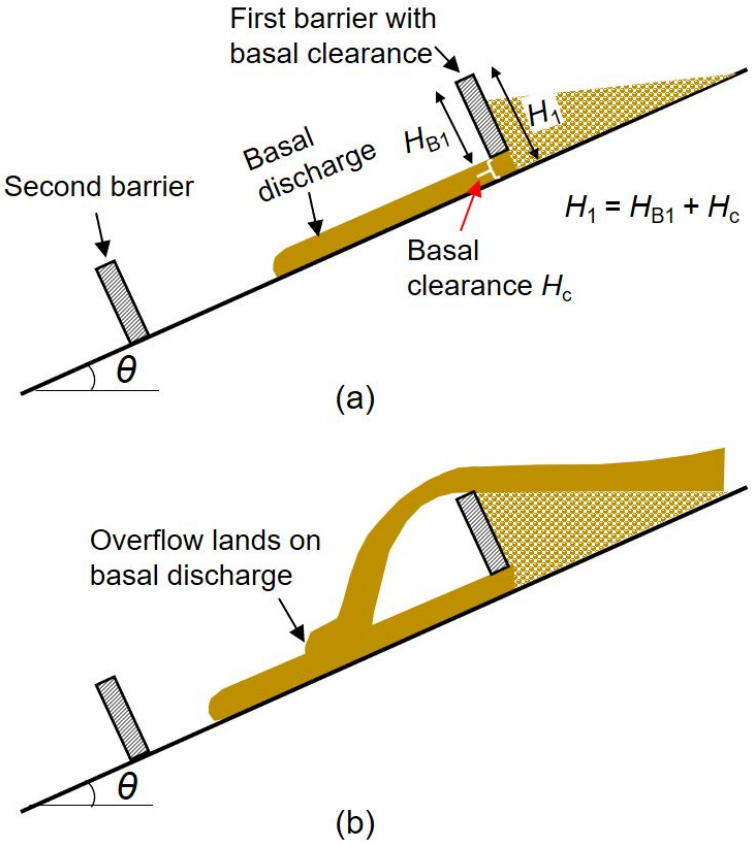

Fig. 2. Schematic of the interaction between flow and dual rigid barriers with a basal clearance beneath the first barrier.

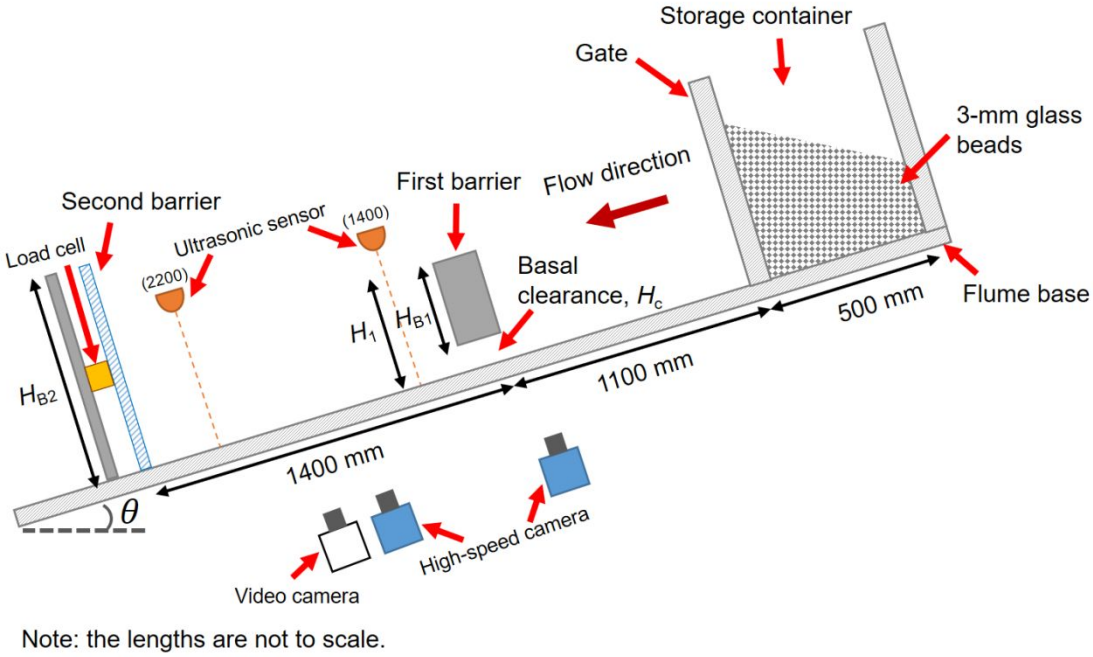

Fig. 3. Schematic of the test set-up and instrumentation.

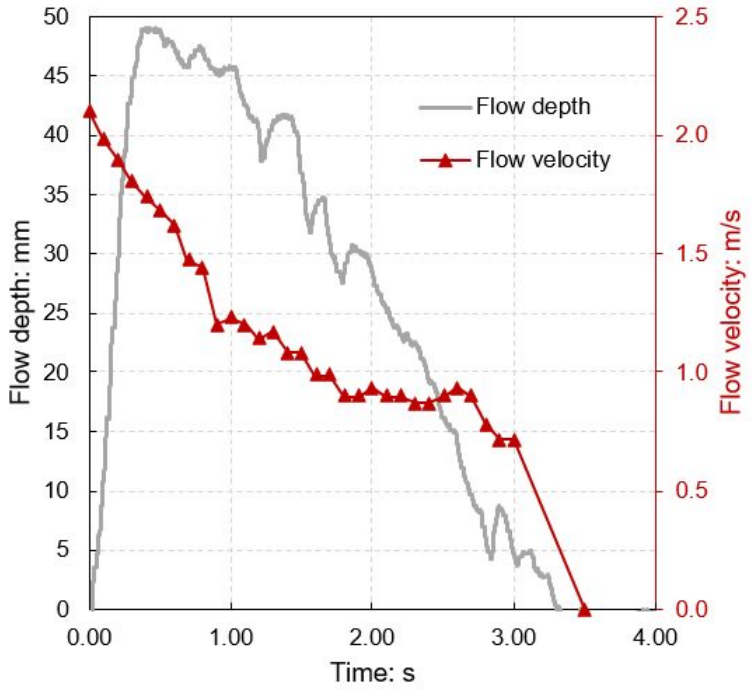

Fig. 4. Time histories of measured flow depth and flow velocity at the first barrier location.

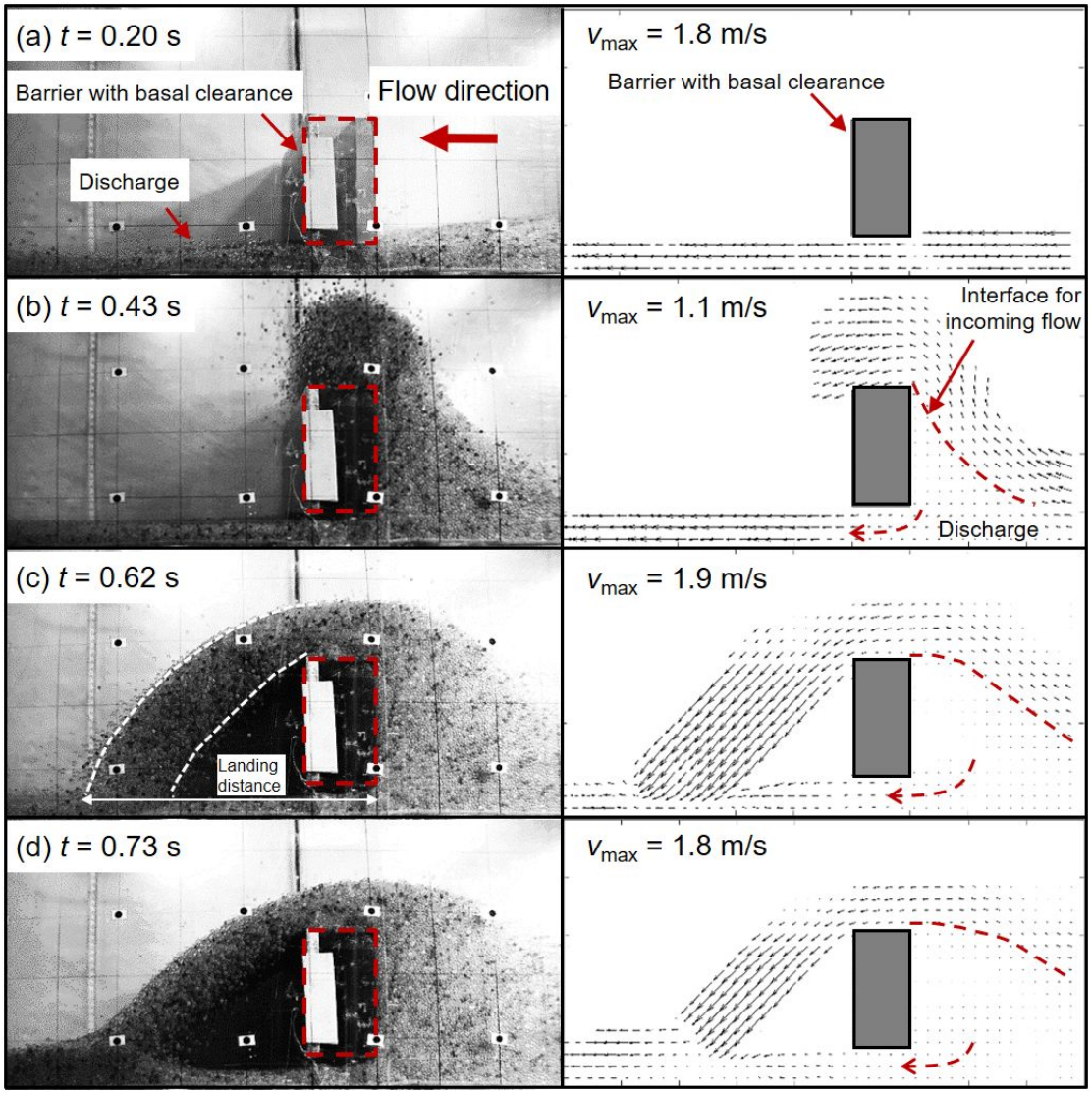

Fig. 5. Observed impact kinematics by high-speed camera (left) and particle image velocimetry (PIV) analysis (right) of test B1C3: (a) $t = 0.20$ s; (b) $t = 0.43$ s; (c) $t = 0.62$ s; (d) $t = 0.73$ s.

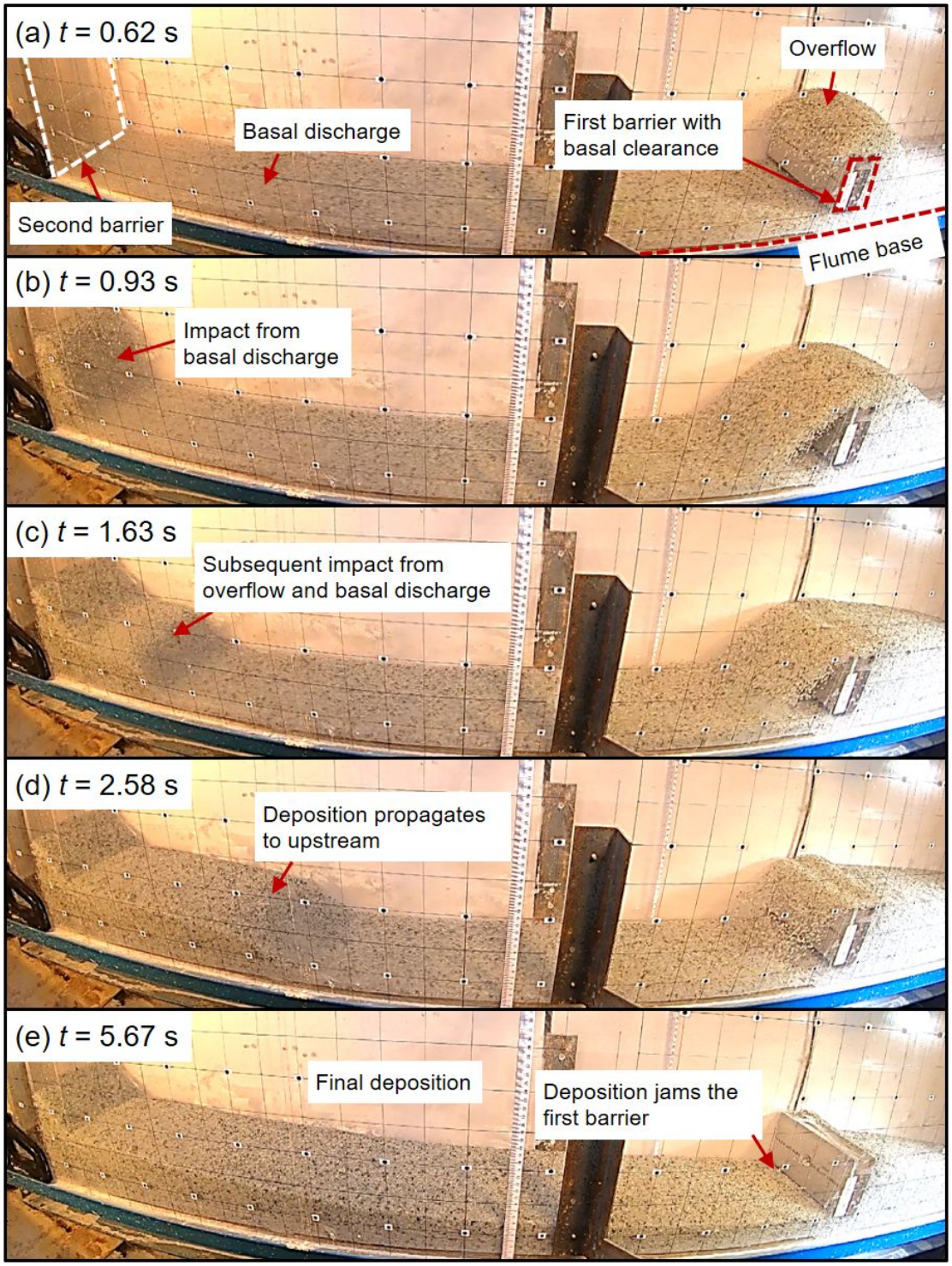

Fig. 6. Observed impact kinematics by video camera of test B1C4: (a) t = 0.62 s; (b) t = 0.93 s; (c) t = 1.63 s; (d) t = 2.58 s; (e) t = 5.67 s.

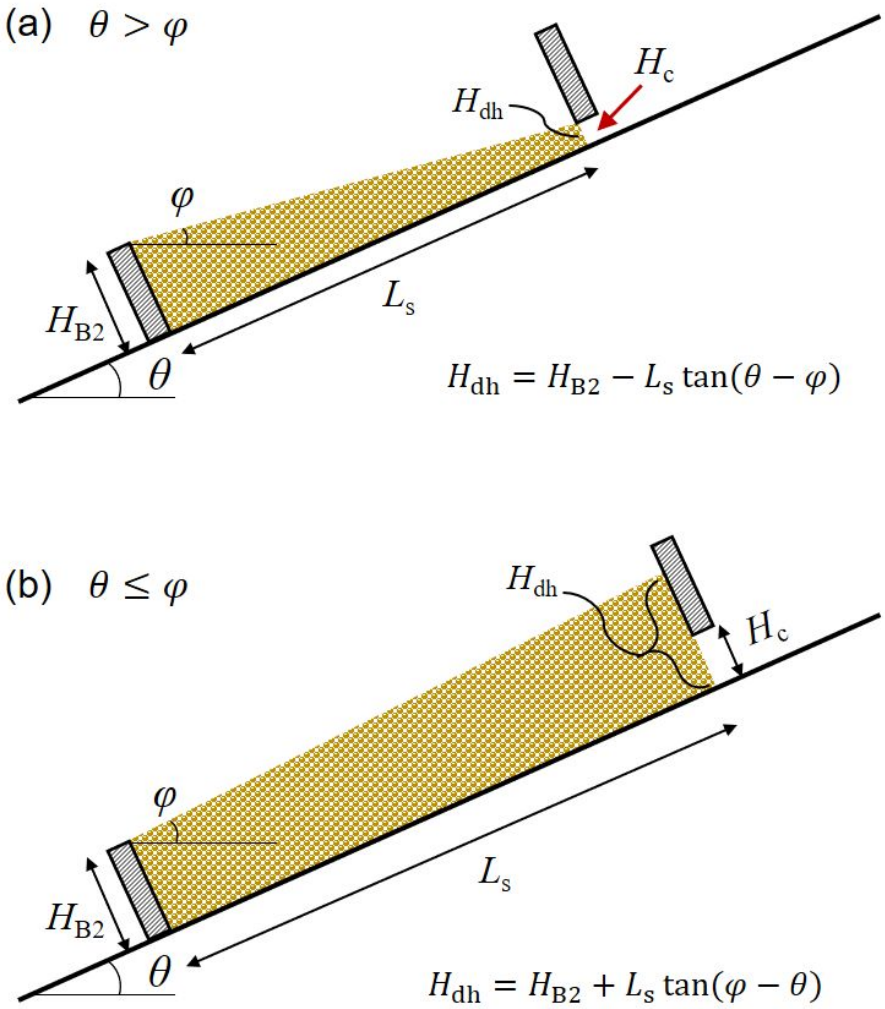

Fig. 7. Schematic of the deposition profiles of the second barrier filled by the flow material with different angles of repose: (a) slope angle larger than angle of repose; (b) slope angle less than or equal to angle of repose.

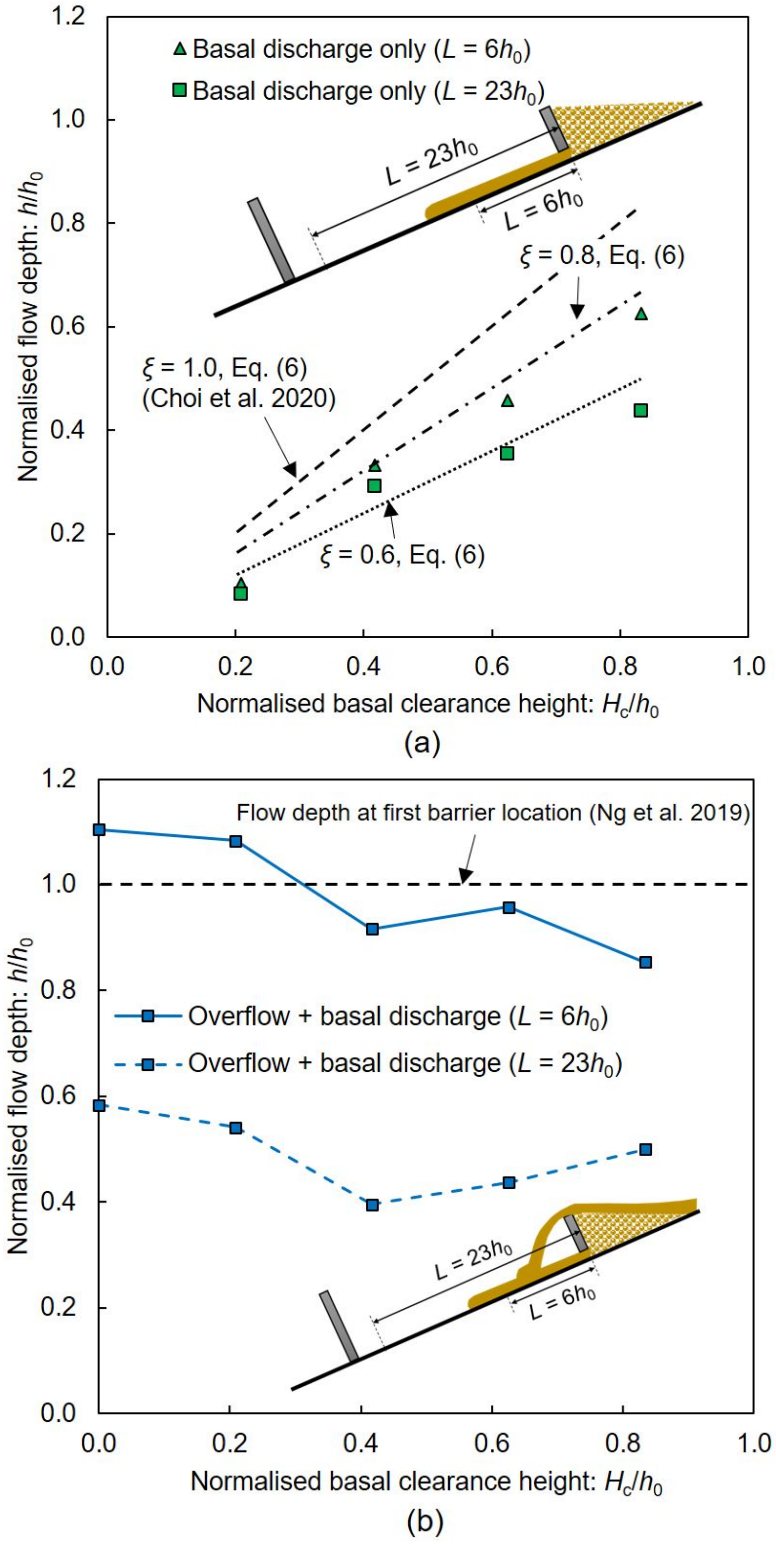

Fig. 8. Comparisons of the measured flow depth downstream the first barrier for different basal clearances: (a) basal discharge; (b) overflow and basal discharge.

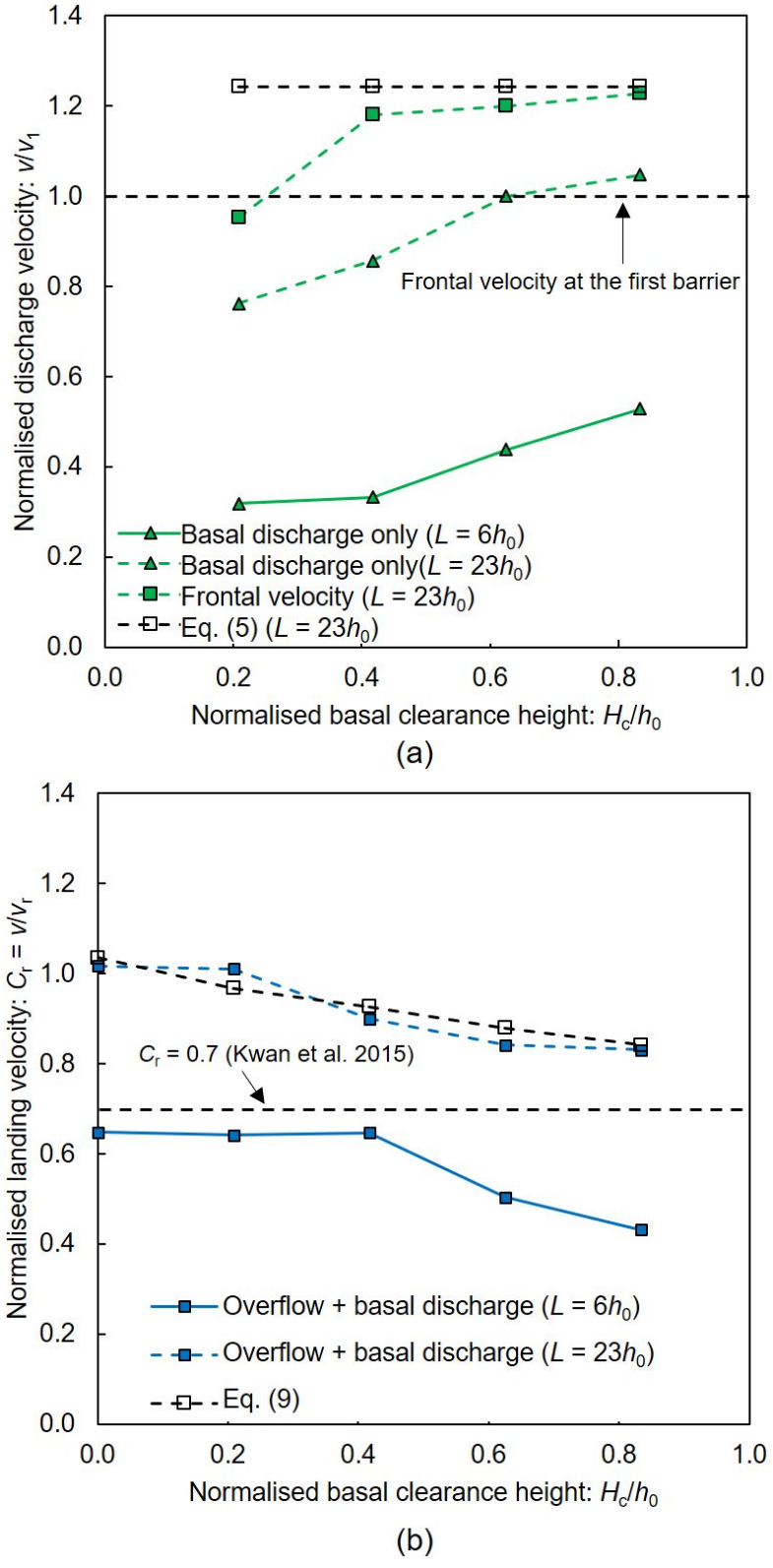

Fig. 9. Comparisons of the measured flow velocity downstream the first barrier for different basal clearances: (a) basal discharge velocity; (b) flow velocity after landing.

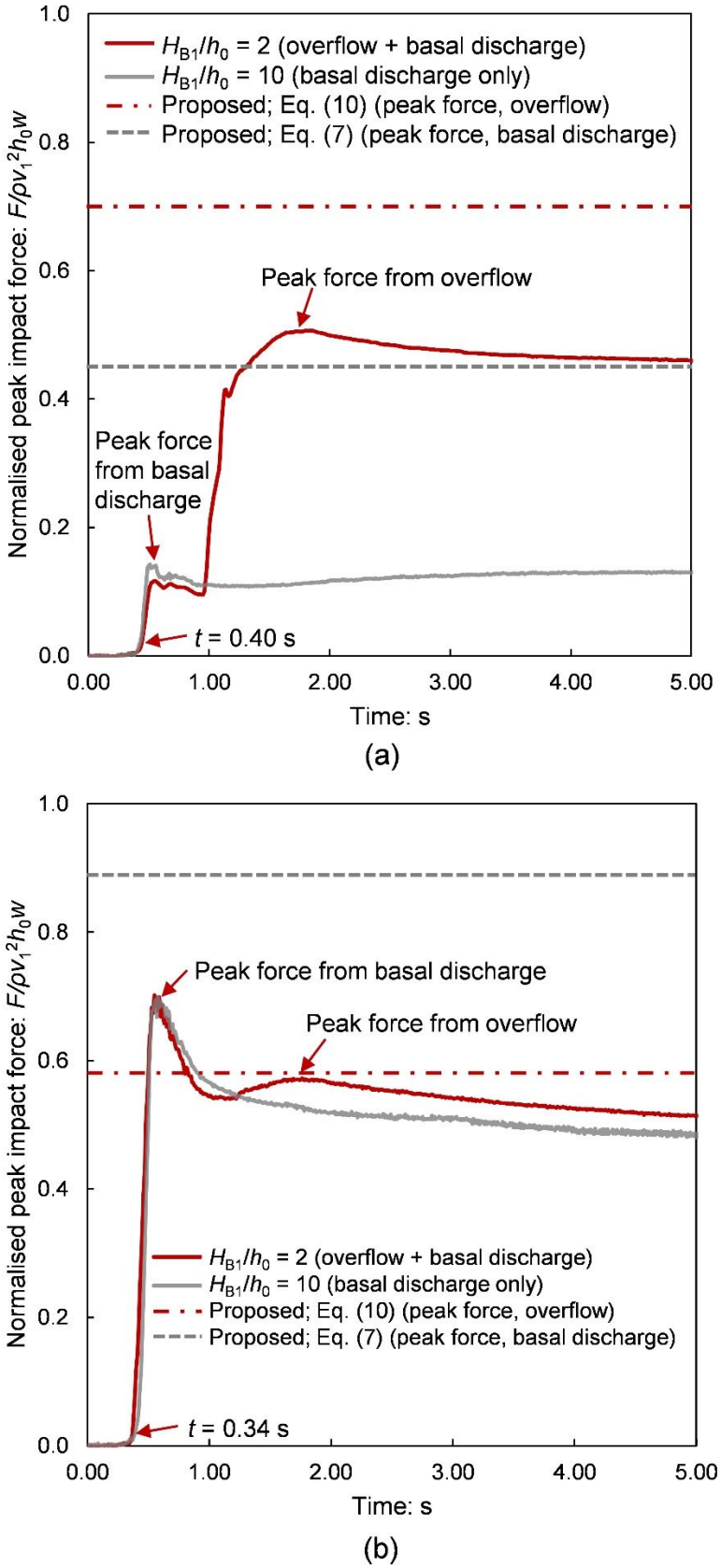

Fig. 10. Time histories of impact force on the second barrier with different basal clearances beneath the first barrier: (a) $H_c/h_0 = 0.4$; (b) $H_c/h_0 = 0.8$.

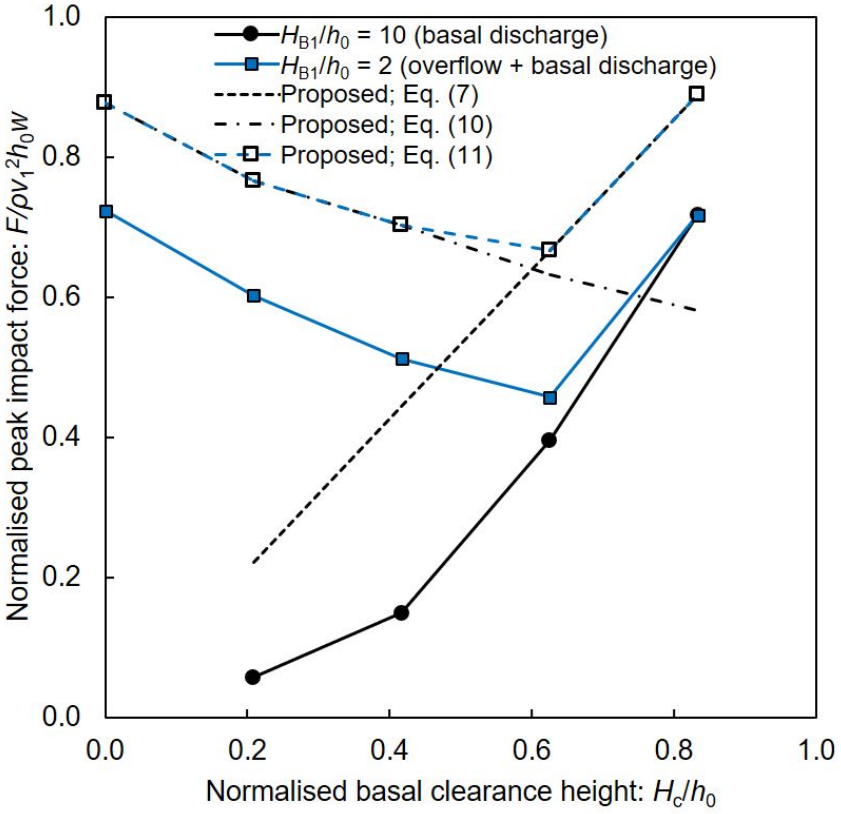

Fig. 11. Comparison of measured and calculated impact forces on the second barrier.